Figure 1. Ellis County, OK tornado of May 4, 2007. Photos courtesy of Reed Timmer and Joel Taylor of TornadoVideos.net. Image (a) is from approximately 1 km away, a few minutes before the viewing at approximately 100 m in the (b) image. Suction vortices are evident at the base of the condensation funnel.

deficit could balance a wind speed of one unit in a surrounding stagnant-core potential vortex.

The grid typically employed $181 \times 181 \times 91$ grid points. The grid is greatly stretched in both the vertical and horizontal. At the surface, the horizontal grid widths $\Delta\ x$ and $\Delta\ y$ are less than 0.0054 in the region $-0.2 < \mathrm{x} < 0.2$ and $-0.2 < \mathrm{y} < 0.2$, where the tornado forms. The grid is stretched in the vertical to enhance the resolution in the viscous boundary layer, leaving $\mathrm{z} = 0.0022$ at the lowest level. The model has fifth-order, upwind-biased advection. An iterative solver maintains a close approximation to incompressibility. As was also done in Fiedler (1998), a companion axisymmetric model in a cylinder, of radius 2 and height 1, is used for comparison with the three-dimensional experiments in a box.

The dimensionless viscosity μ is a constant below $\mathrm{z} = 0.5$, either 4.0×10^{-4}, 1.0×10^{-4} or 2.5×10^{-5}. Above $\mathrm{z} = 0.5$, μ increases linearly to 0.001 at the top boundary at $\mathrm{z} = 1$, to create a damping region in the upper domain. With the height of the domain one unit and the buoyancy-driven velocity scale one unit, μ in the lower half of the domain (the region of interest) could be referred to as the inverse Reynolds number of the simulation. The code allows for interpolation onto a double resolution grid, and restarting of the simulation. For $\mu = 2.5 \times 10^{-5}$, a $361 \times 361 \times 181$ grid sometimes yields suction vortices that are 20% more intense. However, for the two larger μ, there was negligible increase in wind speed at this higher resolution. Some of the statistics reported later for $\mu = 2.5 \times 10^{-5}$ are from these highest-resolution simulations, meaning from a restarted simulation, for a shorter time period of interest. Nevertheless some of the highest wind speed structures reported for $\mu = 2.5 \times 10^{-5}$ are reproducible with either resolution, meaning $181 \times 181 \times 91$ is adequate.

The lower boundary is no-slip, the other boundaries are free-slip. A dimensionless Coriolis force, designated with the usual parameter f, provides the source of the vertical relative vorticity. In the simulations shown here, f varies from 0 to 0.20. Given the width of the simulated vortices is at most 0.1, the Rossby number of these simulations is at least 100. Thus the rotation of the coordinate system is simply a convenient way to provide a source of vertical vorticity that can be stretched and amplified in a central vortex. Except for that, the Coriolis force has negligible effect on the dynamics of the central vortex.

3. Intensity summary

Figure 2 summarizes the minimum pressure $\phi_{\min}$ (pressure divided by density, normalized by velocity scale squared) in the central vortices. The central buoyancy field by itself could sustain $\phi_{\mathrm{hydro}} = -1/2$ at the surface, by hydrostatic means. The ratio of these quantities is plotted as,

$$I_p = \sqrt{\frac{\phi_{\min}}{\phi_{\mathrm{hydro}}}} \tag{1}$$

where I_p, a measure of the intensification of pressure, is being used as in Lewellen and Lewellen (2007a). The statistics are gathered for $t > 100$, well after the initial transient response documented in Fiedler (1998). Statistics from the $361 \times 361 \times 181$ simulations may be for a time interval as small as $\Delta t = 1$, in a simulation restarted by interpolation onto this high resolution grid. Nevertheless, $\Delta t = 1$ allows for several complete orbits of the suction vortex within the parent vortex.

Lewellen and Lewellen (2007a) offer a figure similar to Figure 2, together with a prediction from an analytic model, based on the corner flow swirl ratio S_c. An analysis of Figure 2 is given in the following sections, after a review of S_c.

4. Corner flow swirl ratio

Lewellen *et al.* (2000) introduce a dimensionless parameter, based on properties of the surface boundary

DOI: 10.1002/asl

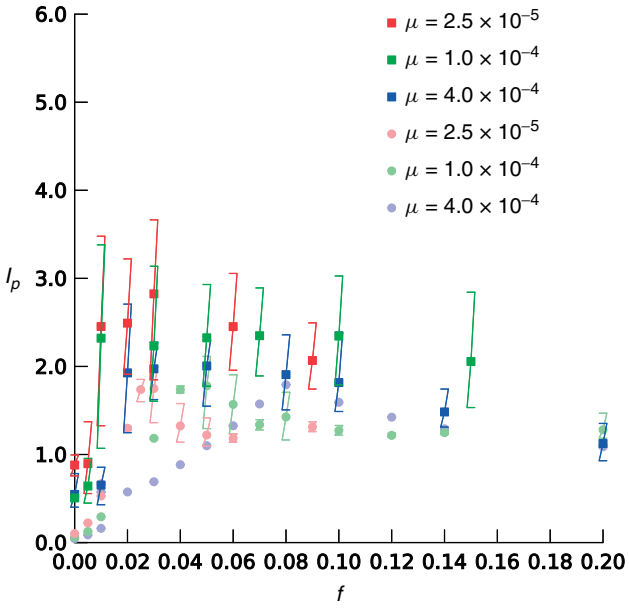

Figure 2. Summary of the maximum pressure deficit I_p in simulations with various dimensionless viscosity μ and dimensionless Coriolis parameter f. Square symbols were three-dimensional simulations within a box. Circular symbols were axisymmetric simulations within a cylinder. 95% of the recorded values are above the low end of the error bar and 5% of the recorded values are above the high end. The central symbol is the mean of the recorded values.

layer flowing into a vortex. The parameter essentially predicts properties of the ensuing central vortex. The parameter is the *corner flow swirl ratio:*

$$S_c = \frac{r_c \Gamma_\infty^2}{\Upsilon} \tag{2}$$

where Γ is the angular momentum, per unit mass, about the center line and Γ_∞ is the ambient value, undisturbed by friction. Υ is the depleted angular momentum flux

$$\Upsilon = -\int_0^{z_1} 2\pi\ r\ u\ (\Gamma_\infty - \Gamma) dz \tag{3}$$

where u is the radial velocity component and the integral is over the depth of the inflowing boundary layer.

The numerator in Equation (2) can be a interpreted as proportional to the *vertical* depleted angular momentum flux in a supercritical flow of maximum intensity. Firstly, r_c is the radius to which fluid with angular momentum of Γ_∞ could penetrate and achieve a swirl velocity V_c:

$$r_c = \frac{\Gamma_\infty}{V_c} \tag{4}$$

where V_c is a dynamical speed limit on the upper portion of the vortex. Secondly, in a loss-free corner flow, the resulting upward velocity component w_c will be proportional to V_c, with a proportionality constant that is in fact the subject of this article. The depleted angular momentum flux up the core will be proportional to $w_c r_c^2 \Gamma_\infty$, or $V_c r_c^2 \Gamma_\infty$, which is the numerator of Equation (2). S_c is thus a measure of the ability of the inflowing boundary layer to adequately supply the core with upward moving fluid depleted of angular momentum, consistent with the constraint on the downstream core size r_c, or equivalently the speed limit V_c.

If S_c is greater than a critical value S_c^*, which Lewellen and Lewellen (2007a) find to be between 0.70 and 1.78, then a high-swirl vortex results, with a central downdraft. If S_c is less than the critical value, then a low-swirl vortex results, with a core wider than r_c and swirl velocity less than allowed by the speed limit V_c. When S_c is at or near the critical value S_c^*, a vortex with strong axial flow can exist, with the strong axial flow terminating in a vortex breakdown close to the surface. This configuration produces the maximum intensity I_p of the vortex (for a given V_c).

The coupling of the inflowing boundary layer to the core of a tornado vortex was also investigated by Fiedler and Rotunno (1986). The boundary layer was that induced by a potential vortex (one with constant Γ_∞ above it) as presented by Burggraf *et al.* (1971), applied at the high Reynolds number limit. From that limit, we can calculate

$$\Upsilon = B\ \delta\ \Gamma_\infty^2 \tag{5}$$

where B = 2.63. δ is the depth of the boundary layer as $r \to 0$:

$$\delta = r_b \sqrt{\frac{\nu}{\Gamma_\infty}} \tag{6}$$

where ν is the kinematic viscosity and r_b is the radius at which the boundary layer begins to form. So from Equations (2) and (5):

$$S_c = \frac{r_c}{B\ \delta} \tag{7}$$

Fiedler and Rotunno (1986) found that the supercritical end-wall vortex that erupts from the boundary layer has a swirl velocity $v_1 = 0.51\ \Gamma_\infty\ \delta^{-1}$. Downstream of the breakdown point $v_2 = 0.25\ \Gamma_\infty\ \delta^{-1}$. (The number 0.25 depending somewhat on assumptions about the distribution of the dissipation). If the flow past the vortex breakdown matches to downstream conditions, or $v_2 = V_c$, then Equation (4) shows $r_c = 4.0\ \delta$. Using these conditions, Equation (7) yields $S_c^* = 1.523$.

More generally, for conditions other than the optimal, combining Equations (6) and (4) with Equation (7) gives:

$$S_c = \Gamma_\infty^{\frac{3}{2}} \nu^{\frac{-1}{2}}\ B^{-1}\ r_b^{-1}\ V_c^{-1} \tag{8}$$

In the dimensionless model, angular momentum is provided by the rotation of the coordinate system, and will have a dimensionless value of $\frac{1}{2} f\ R^2$, where R is the dimensionless radius of the source of fluid

DOI: 10.1002/asl

spatial scales. Monitoring averages from a fixed sampling volume might reveal less of an increase in peak wind speed as Reynolds number increases, but that was not done here.

Putting aside this sampling issue, the results indicate an intensification rule for supercritical vortex flow. Coupling to downstream conditions via a spiral vortex breakdown appears to be quantitatively similar to coupling via a vortex breakdown forced to remain axisymmetric. The three-dimensional simulations have an $I_p \approx 2.5$ (and occasionally much greater than that in transient events) over a broad range of f, while the axisymmetric simulations have $I_p \approx 2.0$, but over a narrow range of f. Such magnitudes of I_p are similar to simulations of Lewellen and Lewellen (2007a), which have parameterized subgrid mixing.

For the present model to simulate the Reynolds number of a thunderstorm, another factor of 10^6 in Reynolds number would be needed. Such simulations may not reveal anything new. These current simulations at low Reynolds number, and those of Lewellen and Lewellen (2007a) at high Reynolds number (with parameterized turbulence), show behavior that is consistent with observations of tornado structure and wind speed near the ground (Bluestein, 2007). Dynamical explanations for tornado structure and wind speed near the ground are not wanting.

Knowledge of S_c, together with knowledge of intensification processes associated with various regimes of S_c, does, in principle, allow for prediction of near-surface tornado intensity. However, acquiring S_c in a tornado event would be operationally more difficult than sensing the intensity itself. There is little, if any time lag, between the appearance of certain value of S_c and the associated intensity. Nevertheless, the science being built upon S_c could have substantial indirect impact on prediction of tornadoes by numerical weather prediction models. For example, such models may forecast well the storm structure and tornadogenesis sites, but otherwise misforecast tornado structure and intensity. This science will provide a focus for a remediation of these models, by directing focus on the model's sensitivity to near-surface turbulence parameterizations and especially the resulting sensitivity of S_c to those parameterizations and to model resolution.

Acknowledgements

This work was supported by National Science Foundation Grant ATM-0646914.

References

Bluestein HB. 2007. Advances in applications of the physics of fluids to severe weather systems. *Reports on Progress in Physics* **70**: 1259–1323, DOI: 10.1088/0034-4885/70/8/R01.

Burggraf OR, Stewartson K, Belcher R. 1971. Boundary layer induced by a potential vortex. *Physics of Fluids* **14**: 1821–1833, DOI:10.1063/1.1693691.

Church CR, Snow JT, Baker GL, Agee EM. 1979. Characteristics of tornado-like vortices as a function of swirl ratio: a laboratory investigation. *Journal of the Atmospheric Sciences* **36**: 1755–1776, DOI: 10.1175/1520-0469(1979)036<1755:COTLVA>2.0.CO;2.

Fiedler BH. 1997. Compressibility and wind speed limits in tornadoes. *Atmosphere-Ocean* **35**: 93–107.

Fiedler BH. 1998. Wind-speed limits in numerically simulated tornadoes with suction vortices. *Quarterly Journal of the Royal Meteorological Society* **124**: 2377–2392, DOI: 10.1002/qj.49712455110.

Fiedler BH, Rotunno R. 1986. A theory for the maximum windspeeds in tornado-like vortices. *Journal of the Atmospheric Sciences* **43**: 2328–2340, DOI: 10.1175/1520-0469(1986)043<2328:ATOTMW>2.0.CO;2.

Fujita TT. 1971. Proposed mechanism of suction spots accompanied by tornadoes. *Preprints, Seventh Conference Severe Local Storms*, Boston, 208–213.

Lewellen DC, Lewellen WS. 2007a. Near-surface intensification of tornado vortices. *Journal of the Atmospheric Sciences* **64**: 2176–2194, DOI: 10.1175/JAS3965.1.

Lewellen DC, Lewellen WS. 2007b. Near-surface vortex intensification through corner flow collapse. *Journal of the Atmospheric Sciences* **64**: 2195–2209, DOI: 10.1175/JAS3966.1.

Lewellen DC, Lewellen WS, Xia J. 2000. The influence of a local swirl ratio on tornado intensification near the surface. *Journal of the Atmospheric Sciences* **57**: 527–544, DOI: 10.1175/1520-0469(2000)057<0527:TIOALS>2.0.CO;2.

Lim TT, Cui YD. 2003. On the generation of a spiral-type vortex breakdown in an enclosed cylindrical container. *Physics of Fluids* **17**: 044105, DOI: 10.1063/1.1872072.

Nolan DS. 2005. A new scaling for tornado-like vortices. *Journal of the Atmospheric Sciences* **62**: 2639–2645, DOI: 10.1175/JAS3461.1.

Serre E, Bontoux P. 2002. Vortex breakdown in a three-dimensional swirling flow. *Journal of Fluid Mechanics* **459**: 347–370, DOI: 10.1017/S0022112002007875.

Xia J, Lewellen WS, Lewellen DC. 2003. Influence of Mach number on tornado corner flow dynamics. *Journal of the Atmospheric Sciences* **60**: 2820–2825, DOI: 10.1175/1520-0469(2003)060<2820:IOMNOT>2.0.CO;2.